



CHORUS

This is the accepted manuscript made available via CHORUS. The article has been published as:

Thermodynamics of Meissner effect and flux pinning
behavior in the bulk of single-crystal
 $\text{La}_{2-x}\text{Sr}_x\text{CuO}_4$ ($x=0.09$)

I. Dhiman, R. Ziesche, V. K. Anand, L. Riik, Gian Song, A. T. M. N. Islam, Isao Tanaka, and
W. Treimer

Phys. Rev. B **96**, 104517 — Published 28 September 2017

DOI: [10.1103/PhysRevB.96.104517](https://doi.org/10.1103/PhysRevB.96.104517)

Thermodynamics of Meissner effect and flux pinning behavior in the bulk of single crystal $\text{La}_{2-x}\text{Sr}_x\text{CuO}_4$ ($x = 0.09$)

I. Dhiman,^{1,2,*} R. Ziesche,^{2,3} V. K. Anand,² L. Riik,^{2,4} Gian Song,¹ A. T. M. N. Islam,² Isao Tanaka,⁵ and W. Treimer^{2,4}

¹*Chemical and Engineering Materials Division, Oak Ridge National Laboratory, Oak Ridge, Tennessee 37831, USA*

²*Helmholtz-Zentrum Berlin für Materialien und Energie GmbH, Hahn-Meiter Platz 1, D-14109 Berlin, Germany*

³*Department of Chemical Engineering, University College London, Torrington Place, London WC1E 7JE, UK*

⁴*University of Applied Sciences Berlin Beuth Hochschule für Technik Berlin, D 13353 Berlin, Germany*

⁵*Center for Crystal Science and Technology, University of Yamanashi,*

7-32 Miyamae, Kofu, Yamanashi 4008511, Japan

We have studied the evolution of magnetic flux pinning behavior in the Meissner phase and the mixed state for the high- T_c single crystal $\text{La}_{2-x}\text{Sr}_x\text{CuO}_4$ ($x = 0.09$) superconductor using the polarized neutron imaging method with varying magnetic field and temperature. In the Meissner state expulsion of magnetic field (switched on during the measurements) is visualized, and the signatures of mixed state with increasing temperature are observed. While, for flux pinning behavior between $5 \text{ K} \leq T \leq 15 \text{ K}$ and $H_{\text{ext}} = 63.5 \text{ mT}$ (switched off during the measurements), the evolution of fringe pattern indicates magnetic flux pinning inside the bulk of the sample. At $25 \text{ K} \leq T \leq 32 \text{ K}$, a continuous decrease of inhomogeneously distribution pinned magnetic flux is observed, with the sample reaching a normal conducting state at T_c ($\approx 32 \text{ K}$). The flux pinning behavior is also explored as a function of H_{ext} , at $T = 5 \text{ K}$. As expected, with increasing H_{ext} an increase in fringe density is observed, indicating an increase in magnetic flux pinning in the bulk of the sample. Comparison between calculated and experimentally visualized pinned magnetic flux shows good agreement. This implies quantification of pinned magnetic flux inside the sample, which is not possible with any other technique on bulk samples.

Notice of Copyright

Manuscript has been authored by UT-Battelle, LLC under Contract No. DE-AC05-00OR22725 with the U.S. Department of Energy. The United States Government retains and the publisher, by accepting the article for publication, acknowledges that the United States Government retains a non-exclusive, paid-up, irrevocable, worldwide license to publish or reproduce the published form of this manuscript, or allow others to do so, for United States Government purposes. The Department of Energy will provide public access to these results of federally sponsored research in accordance with the DOE Public Access Plan (<http://energy.gov/downloads/doe-public-access-plan>)

I. INTRODUCTION

Since the discovery of high- T_c superconductivity in doped cuprates, the nature and understanding of superconductivity in these materials have been a subject of substantial interest, owing to their intriguing properties and high transition temperatures (T_c)¹⁻⁸. $\text{La}_{2-x}\text{Sr}_x\text{CuO}_4$ is one such high- T_c superconductor, a prototype material for investigations and understanding of superconductivity in the family of cuprates^{1,7,9-11}. The $\text{La}_{2-x}\text{Sr}_x\text{CuO}_4$ series exhibits several thermodynamic phases depending on the degree of doping and oxygen content. The stoichiometric undoped parent compound La_2CuO_4 is an antiferromagnetic insulator with a Néel temperature $T_N \approx 320 \text{ K}$ for the order-

ing of Cu^{2+} moments¹². Substituting divalent Sr with trivalent La, or the presence of excess oxygen, leads to hole doping, causing suppression of long range ordered antiferromagnetism¹³⁻¹⁹. A nominal substitution of 2% Sr ($x = 0.02$) completely suppresses the antiferromagnetic ordering in $\text{La}_{2-x}\text{Sr}_x\text{CuO}_4$ ^{19,20}, whereas a superconducting state appears at $x \geq 0.055$ with a maximum T_c for $x = 0.15$. With a type-II behavior these high- T_c superconductors present an intriguing vortex phase²¹⁻²⁵.

Understanding of the flux pinning behavior is important not only from the viewpoint of physics, but also for technological relevance, as this is the mechanism involved to enhance critical current values in type-II superconductors²⁶⁻³¹. For most applications it is extremely desirable to control pinning effects, and the related current densities. To obtain an insight into the mixed state flux pinning behavior and complex interplay of superconductivity with magnetism in these systems, several studies, in particular neutron scattering based measurements³²⁻⁴⁷ in reciprocal space and various surface based imaging techniques in real space, have been performed. The vortex lattice structures in superconductors are also investigated with small angle neutron scattering (SANS) technique⁴⁸⁻⁵³. However, the neutron scattering averages through the whole sample, the information about the inhomogeneous vortex lattice structures is not resolved.

The surface based scanning tunneling microscopy (STM) technique has been extensively used for the study of superconducting vortices, particularly for the high- T_c $\text{Bi}_2\text{Sr}_2\text{CaCu}_2\text{O}_{8+\delta}$ and $\text{YBa}_2\text{Cu}_3\text{O}_7$ cuprates⁵⁴⁻⁵⁹. The major challenge with STM is to have atomically

flat/stable and extremely clean surfaces. Another technique utilized towards the visualization of magnetic flux distribution is magneto-optical imaging^{56,60–63}. In this method the local super-current density distribution is mapped in thin superconducting films, with out of plane component sensitivity and spatial resolution of the order of $5 \mu\text{m}$. Further, scanning SQUID^{56,64}, time resolved Lorentz microscopy imaging^{65–69}, magnetic force and scanning hall probe microscopy^(56, and references therein) based techniques have also been used to study the interactions, flux lattice dynamics, and geometries of vortices in multiband superconductors. These techniques indeed provide high resolution images, however, the information obtained stems from rather two-dimensional objects, providing insight into superconducting mixed states on the surface.

The polarized neutron imaging technique on the other hand provides a unique probe for the visualization of the magnetic field in and around the bulk of a sample, therefore making a substantial contribution in the field of superconductivity and magnetism⁷⁰. Flux pinning in $\text{La}_{2-x}\text{Sr}_x\text{CuO}_4$ systems have been previously investigated by Kishio *et al.*⁷¹ for $x = 0.065$ and 0.07 using magnetization measurements. However, in this technique one has to deal with the undesirable demagnetization effects. In contrast, with polarized neutron imaging technique flux pinning behavior can be visualized in the bulk samples; therefore the demagnetization effect does not have any direct bearing on the flux pinning behavior. Furthermore, with magnetization measurement technique one cannot visualize magnetic field expulsion or flux pinning in real space. The polarized neutron imaging technique makes this visualization possible.

In the current study, it is of interest to investigate and understand the complex interplay of flux pinning phenomenon and Meissner behavior in the mixed state, as a function of temperature and externally applied magnetic field (H_{ext}) in the bulk of underdoped $\text{La}_{2-x}\text{Sr}_x\text{CuO}_4$ ($x = 0.09$) single crystal sample using novel real space polarized neutron imaging technique. In addition, the real-space visualization of magnetic domain structures has been so far limited to surface-sensitive techniques. While, neutrons can easily penetrate bulk samples and due to their magnetic moment can interact with the local magnetic field distributions. Recently, this technique has been recognized as a powerful non-destructive tool to visualize the magnetic field distribution in various ferromagnetic samples and pinned flux in superconductors^{72–77}. From a macroscopic viewpoint, the superconducting state is a thermodynamic phase. Involving temperature and magnetic field as an external variable is an effective way to understand the evolution of flux pinning behavior in bulk samples.

II. THEORETICAL CONSIDERATION

Visualization of magnetic field using polarized neutrons is based on the neutron spin interaction with the magnetic field in the bulk samples. The neutron spin interacts with the magnetic field B (in / around the sample), rotating around B with a Larmor frequency $\omega_L = \gamma_L B$, where $\gamma_L = g\mu_N\hbar = -1.832 \times 10^8 \text{ rad s}^{-1} \text{ T}^{-1}$ is the gyromagnetic ratio of the neutron, $\mu_N = 5.5078 \times 10^{-27} \text{ J/T}$ is the nuclear magneton and $g = -3.8261$ is the Landé factor for neutrons, h ($\hbar = \frac{h}{2\pi}$) is the Planck constant. If the neutron spin interacts with a magnetic field B , which is not parallel or anti-parallel to its spin direction, it begins to make Larmor precession with the frequency ω_L . The rotation angle ϕ of the neutron spin is dependent on the time t taken by neutrons to pass through magnetic field. The ϕ can be calculated as,

$$\phi = \omega_L t = \gamma_L B t = \frac{\gamma_L}{\nu} \int_{\text{path}} \vec{B} \cdot d\vec{s} = \frac{\gamma_L \cdot \lambda \cdot m}{h} \cdot B \cdot s \quad (1)$$

where ‘ m ’ is the neutron mass, ‘ s ’ is path integral in the field, ν ($= \frac{h}{m \cdot \lambda}$) is the neutron velocity, and λ is the wavelength. The integration limit for pinned flux is defined by sample dimensions and is dependent on the amount of magnetic field B .

III. EXPERIMENTAL DETAILS

Single crystal growth of $\text{La}_{2-x}\text{Sr}_x\text{CuO}_4$ ($x = 0.09$) was carried out in a four-mirror type optical image furnace (Crystal Systems Corp., Japan) by the traveling-solvent-floating-zone technique. We used oriented crystal as seed rod which enabled an epitaxial growth of crystal along the [010] direction. This way we could obtain an oriented crystal of almost cylindrical geometry with the cylindrical axis along the crystallographic [010] direction. The composition of the single crystal was determined by electron-probe-microanalysis (EPMA) using a standard sample. X-ray Laue diffraction was used to check the quality of the as-grown single crystal and to orient the crystal along the particular crystallographic direction. The magnetic susceptibility measurements were performed using Quantum Design superconducting quantum interference device vibration sample magnetometer (SQUID-VSM) at the Mag Lab, Helmholtz-Zentrum Berlin.

The polarized neutron imaging measurements were performed on instrument PONTO II (POLarized Neutron TOMography) located at BER II (Berlin research reactor) of the Helmholtz Zentrum Berlin für Materialien und Energie, in neutron guide hall at NL1a beam port. It is dedicated for radiography and tomography studies using polarized neutrons, covering a wavelength range of $0.29 \text{ nm} < \lambda < 0.45 \text{ nm}$ using a graphite monochromator ((002), reflection). The detailed description of the instrument can be found in ref.⁷⁸. For the

present study, the graphite monochromator was positioned so as to reflect a mean wavelength of 0.32(1) nm towards an optical bench. Soller collimators were utilized for both horizontal and vertical collimation of the beam with 0.1° divergence. For beam polarization (spin analysis) a bender type polarizer (analyzer) was used, providing polarization degree of $P=92\%$. Neutron flux at the sample position was 3.2×10^6 neutrons $\text{cm}^{-2}\text{s}^{-1}$, with a field of view of 40×40 mm^2 and the obtained 2D spatial resolution for polarized neutrons was 130 μm . The detector unit comprised a LiZnS scintillator, Nikon objective and Andor CCD camera with a pixel array of $2 \text{ k} \times 2 \text{ k}$ (each pixel size = 13.6 $\mu\text{m} \times 13.6 \mu\text{m}$). The sample was placed in an aluminum sample holder, which was screwed to the cold finger of a closed cycle refrigerator, and could be rotated by $360 (\pm 0.005)^\circ$. A homogeneous external magnetic field ($= H_{\text{ext}}$) was applied using a pair of Helmholtz coils at the sample position. The exposure time for each radiograph was 2 hrs.

With polarized neutron imaging, the measured transmission intensity is a sum of the contribution from the interaction of the neutron spin with the sample magnetic field, the conventional attenuation (depending on sample composition- and density) and scattering. To remove the conventional attenuation and scattering contribution, radiographs were normalized with respect to the radiographs measured with no magnetic contribution, in the normal conducting state for $T > T_c$. This is particularly important for small magnetic field contributions. All the neutron radiographs recorded were corrected for dark field, the constant background/electronic noise from the detector and normalized with respect to the radiographs recorded at 50 K, above T_c (≈ 31.65 K).

The sample was approximately cylindrical in shape with dimensions of radius = 2.4 mm and height = 5.8 mm. To visualize the flux pinning behavior, field cooling (FC) was employed. First the sample was cooled to 50 K in one step. After a waiting time of nearly 1 hour, two hours polarized neutron radiography measurements were performed at $T = 50$ K ($T > T_c$). After this a homogeneous external magnetic field ($= H_{\text{ext}}$) was applied and the sample was cooled down to 5 K. At 5 K, the external magnetic field ($H_{\text{ext}} = 0$) was switched off, so as to investigate the flux pinning behavior. Now, again radiographs were recorded at various temperature steps up to 32 K, just above T_c . For all the measurements reported here the external magnetic field was applied along 0° orientation, i. e. for sample axis orientation parallel to the external magnetic field (as shown in Fig. 1). Whereas, for the visualization of the Meissner effect sample was zero field cooled to 5 K. Thereafter, magnetic field was switched on and radiographs were measured in steps while warming the sample from 5 K to 32 K ($T > T_c$).

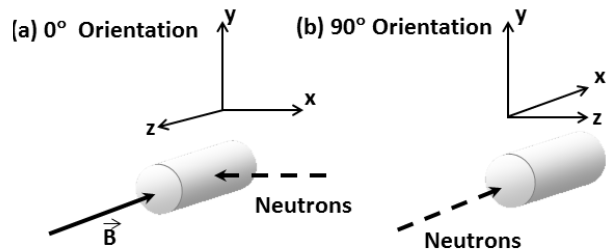


FIG. 1: Sample orientation with respect to the incident neutrons, wherein for (a) 0° orientation sample axis is perpendicular to the incident neutrons. While for (b) 90° orientation sample axis is parallel to the incident neutrons. To visualize flux pinning behavior in 90° orientation, first the sample is cooled down to 5 K with $H_{\text{ext}} = 63.5$ mT along the direction parallel to the sample axis, i. e. in 0° position. Thereafter H_{ext} is switched off and sample is turned to 90° position.

IV. RESULTS AND DISCUSSION

A. Magnetization behavior

To determine the T_c for $\text{La}_{2-x}\text{Sr}_x\text{CuO}_4$ ($x = 0.09$) sample, magnetization measurements as a function of temperature were carried out. The temperature dependent volumetric magnetic susceptibility plots are shown in figure 2. The temperature dependent magnetization data is obtained with zero field cooled warming the sample, in the presence of external magnetic field ($H_{\text{ext}} = 20$ and 50 mT). The superconducting transition temperature for $\text{La}_{2-x}\text{Sr}_x\text{CuO}_4$ ($x = 0.09$) sample is ≈ 32.05 K for $H_{\text{ext}} = 20$ mT. Below this temperature, the sample displays Meissner response, with strong diamagnetic signal. A small decrease in critical temperature, T_c ($= 31.65$ K), is observed on increasing H_{ext} to 50 mT. An indirect estimate of the superconducting phase fraction is obtained from the magnetization data. The demagnetization factor for perfect cylindrical geometry has been taken into consideration to estimate the superconducting volume fraction⁷⁹. The obtained volumetric fraction is nearly 100 %, for 20 mT at $T = 5$ K. As expected, this value is reduced to $\approx 91\%$ for higher magnetic field of 50 mT. However, with magnetization measurements no information about the flux pinning behavior can be obtained in the bulk of the sample. The magnetization behavior is in agreement with the reported for $\text{La}_{2-x}\text{Sr}_x\text{CuO}_4$ series in literature¹⁴.

Based on these initial magnetization results, the polarized neutron imaging measurements as a function of temperature were carried out on cylindrical shaped $\text{La}_{2-x}\text{Sr}_x\text{CuO}_4$ ($x = 0.09$) single crystal sample. In the Meissner phase (for $T < T_c$), the expelled magnetic field is visualized as the superposition of expelled magnetic field and H_{ext} . On the other hand, flux pinning behavior leads to an evolution of pinned flux lines/pattern inside the sample, as discussed in greater detail below. Assuming that polarizer and analyzer are configured for spin

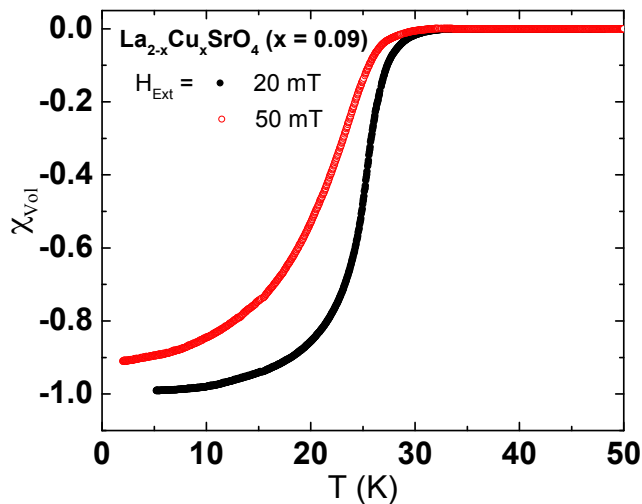


FIG. 2: Volumetric magnetic susceptibility as a function of temperature at $H_{\text{ext}} = 20$ mT (closed circle symbol) and 50 mT (open circle symbol) for $\text{La}_{2-x}\text{Sr}_x\text{CuO}_4$ ($x = 0.09$) single crystal sample.

up neutrons, and for strong enough magnetic field of the sample the out going neutron spin is rotated i. e. making a π -flip. This would cause minimum transmission (for ideal set-up) intensity measured on the detector placed behind the analyzer. Now if the analyzer is modified

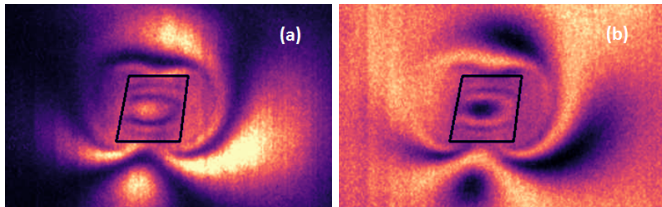


FIG. 3: Representative radiographs for single crystal $\text{La}_{2-x}\text{Sr}_x\text{CuO}_4$ ($x = 0.09$) sample at 5 K and $H_{\text{ext}} = 30$ mT for 0° orientation, depicting the fringe patterns with (a) spin down (dark) and (b) spin up (bright) neutrons. The black box indicates the sample cross section.

to accept only spin down neutrons (π -flip), inversion in transmission intensity contrast, i. e. maximum transmission is measured on the detector. All the other neutron spin precession values between 0 and π will lead to grey value contrast, dependent on the total degree of polarization and instrument resolution. Representative radiographs exhibiting the flux pinning behavior below the T_c are shown in figure 3. The two radiographs shown are recorded with spin up and down incident neutrons, causing change in contrast (bright to dark). The alteration of fringe pattern intensity from dark to bright corresponds to a spin rotation of π (π -flip), implying the magnetic nature of these fringes. Each individual fringe in the figure represents that all the incoming polarized neutrons

experience same path integral ($\int_{\text{path}} \vec{B} \cdot d\vec{s}$) change.

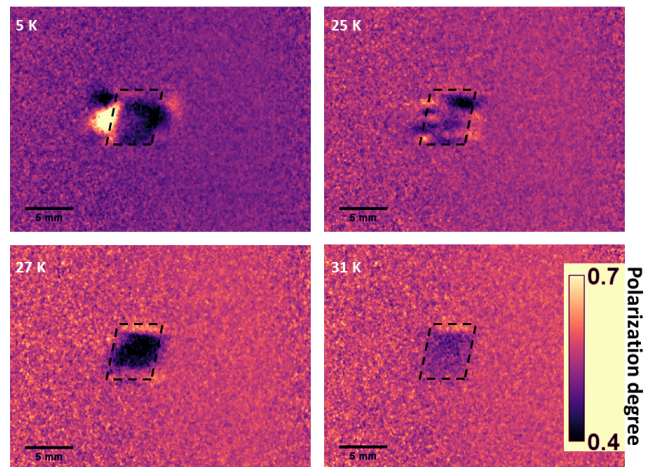


FIG. 4: Meissner effect as a function of temperature at $H_{\text{ext}} = 10$ mT, for single crystal $\text{La}_{2-x}\text{Sr}_x\text{CuO}_4$ ($x = 0.09$) sample below T_c . For these measurements, sample is cooled down to 5 K from room temperature with $H_{\text{ext}} = 0$ mT. At 5 K to visualize Meissner effect, H_{ext} is set to 10 mT. The black dashed box indicates the sample and scale bar is 5 mm.

B. Meissner effect

In figure 4, neutron radiographs show temperature dependence of Meissner effect in the presence of external magnetic field. Sample is cooled down to 5 K below T_c , with $H_{\text{ext}} = 0$ mT. Then the magnetic field is applied to the sample. As observed in figure 4 for $T < T_c$ at $H_{\text{ext}} = 10$ mT, a dark pattern appears around the sample, indicating expulsion of magnetic field. As a function of increasing temperature, a weak signature of mixed state is observed. Wherein, the expelled magnetic flux begins to penetrate, in agreement with the change in transmission contrast inside (dark pattern) and outside (bright pattern) the sample. This contrast indicates the difference in magnitude of stray field in and around the sample. At 27 K, the bright pattern outside the sample is reduced, indicating the weakening of Meissner effect. On further increasing the temperature $T \geq T_c$, the pattern disappears with sample reaching a normal state. Therefore one recognizes the evolution of mixed state, with changes in pinned and expelled magnetic flux in and around the sample, as a function of temperature.

C. Flux pinning behavior as a function of Temperature

In a normal non-superconducting state for $T > T_c$, applied magnetic field penetrates the whole sample. Now when the sample is field cooled below T_c , this applied

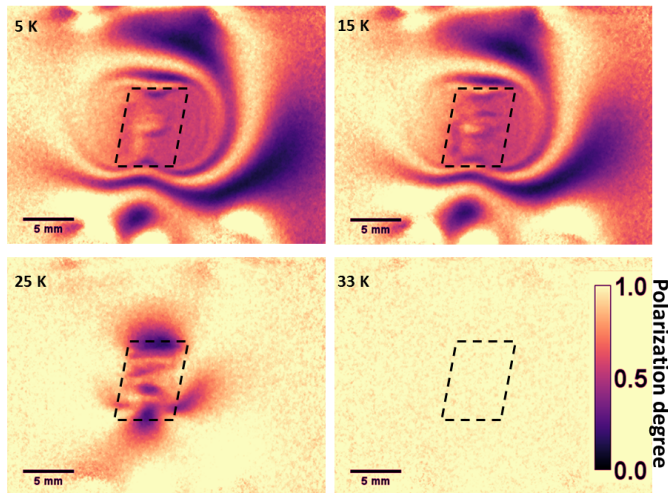


FIG. 5: Temperature dependence of flux pinning behavior at $H_{\text{ext}} = 63.5$ mT for 0° orientation, for single crystal $\text{La}_{2-x}\text{Sr}_x\text{CuO}_4$ ($x = 0.09$) sample. Towards these measurements, sample is cooled down to 5 K from room temperature, in the presence of H_{ext} . Thereafter, to visualize flux pinning, external magnetic field is switched off. Consequently, any depolarization of neutrons spin can be attributed to the flux pinned within the sample. The black dashed box indicates the sample and scale bar is 5 mm.

field is expected to be expelled. At 5 K, with H_{ext} switched off no magnetic contrast is expected inside the sample. Contrastively, in the present study fringe pattern is evolved for $T < T_c$ at 5 K for $\text{La}_{2-x}\text{Sr}_x\text{CuO}_4$ ($x = 0.09$) single crystal sample. Figure 5 shows the measured radiographs in 0° orientation (see figure 1(a)) for $\text{La}_{2-x}\text{Sr}_x\text{CuO}_4$ ($x = 0.09$) single crystal sample as a function of temperature, exhibiting signature of the flux pinning behavior. Towards these measurements, sample is cooled down to 5 K in the presence of external magnetic field ($H_{\text{ext}} = 63.5$ mT). Thereafter, H_{ext} is switched off. Any change in incident neutron spin rotation must be attributable to the flux pinned in the sample. Consequently, the temperature dependent behavior in the present study is entirely a sample phenomenon. In figure 5, evolution of the closed loop type (outside the sample) fringe pattern at $T = 5$ and 15 K is observed. Appearance of this fringe pattern for $T < T_c$ clearly indicates the flux pinning behavior inside the sample. Also, for $T = 5$ and 15 K fringes located close to the longitudinal axis appear higher in intensity (figure 5), and diminish on moving towards the sample edge. This behavior implies maximum neutron spin precession around the longitudinal axis. This in turn indicates that the magnetic flux is concentrated around that axis, and reduces on moving away towards the edge. This effect is further enhanced due to different neutron path length through the cylindrical shaped sample. This behavior is in corroboration with our previously reported studies on type-I Pb

superconductor^{76,77}. This distribution can only occur for a magnetic field which appears to be squeezed around the rod axis, i.e. it has a Gaussian-like distribution inside the sample. Detailed calculations pertaining to this can be found in reference⁷⁶. At $T = 25$ K, deviation from this Gaussian distribution is observed and concentration fluctuations in flux pinning behavior at temperatures close to T_c is ascertained. This deviation is visualized more clearly for 90° sample orientation, in figure 7 below. To

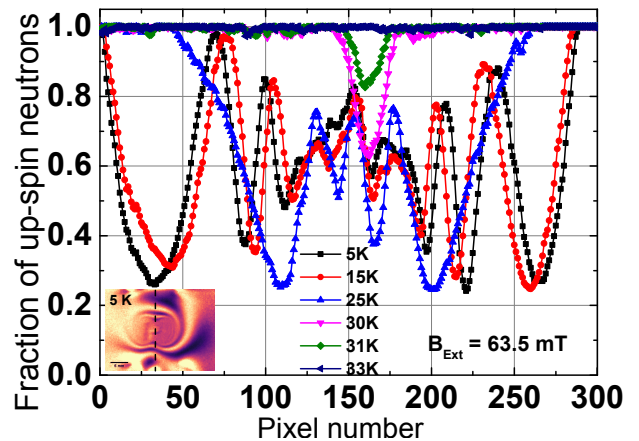


FIG. 6: Line plots to depict the temperature dependence of flux pinning behavior from 5 K to 33 K, for single crystal $\text{La}_{2-x}\text{Sr}_x\text{CuO}_4$ ($x = 0.09$) sample in 0° orientation, $H_{\text{ext}} = 63.5$ mT. The inset radiograph shows an example of vertical line used for the plot. Each pixel number corresponds to 78 μm .

graphically visualize the effect of temperature, line plots as a function of temperature are presented in figure 6. Towards this, a vertical line is drawn in each radiograph where the fringe pattern is quite horizontal, as shown in the inset to figure 6. Same procedure is repeated for all the radiographs. With varying temperature a clear reduction in intensity is evidenced above $T = 25$ K, in corroboration with the reduction in pinned magnetic field as a function of temperature. This behavior indicates strong temperature dependence of pinned flux inside the sample above 25 K.

Figure 7 shows the temperature dependence of flux pinning behavior in 90° orientation for $\text{La}_{2-x}\text{Sr}_x\text{CuO}_4$ ($x = 0.09$) single crystal. At 5 K to visualize flux pinning behavior in 90° sample orientation, H_{ext} is switched off and sample is turned to 90° position, as shown in figure 1. Ring shaped fringe pattern is observed at $T = 5$ K, depicted in figure 7. This is in corroboration with the observed stripe shaped fringe pattern in 0° orientation. Collective visualization of this expected behavior in 0° and 90° orientation, can be clearly deciphered on comparison with the modelled magnetic field distribution in 3D for cylindrical shaped sample described by Treimer *et al.* in ref.⁷⁶. The temperature evolution of the flux pin-

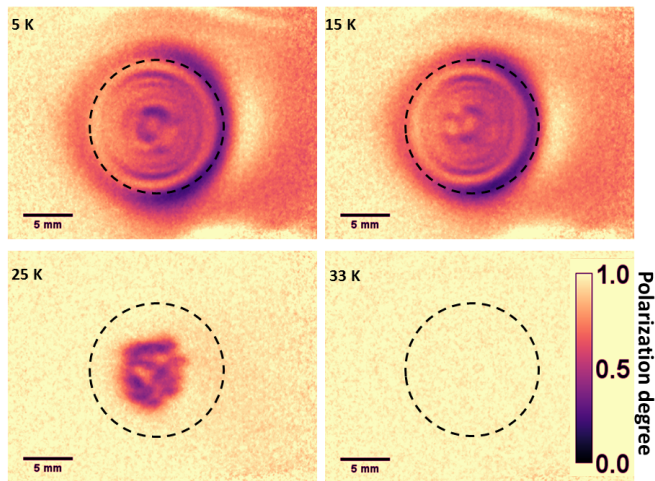


FIG. 7: Flux pinning behavior as a function of temperature for 90° sample orientation, for single crystal $\text{La}_{2-x}\text{Sr}_x\text{CuO}_4$ ($x = 0.09$) sample. For these measurements, sample is cooled down to 5 K with $H_{\text{ext}} = 63.5$ mT applied in 0° position. At 5 K to visualize flux pinning behavior for 90° sample orientation, first H_{ext} is switched off, and then the sample is turned to 90° position. The black dashed circle indicates the sample and scale bar is 5 mm. Note the decrease of pinned flux with increasing temperature.

ning in 90° sample orientation exhibits behavior similar to that described for 0° orientation. In particular, radiograph measured at 25 K exhibits inhomogeneous flux distribution, with parts in the sample where flux lines are closer to each other (more concentrated) than in other regions. This behavior indicates deviation from Gaussian distribution and fluctuations in pinned flux on increasing the temperature close to T_c .

The evolution of fringe pattern with varying temperature, below the critical temperature can be argued to arise from two possibilities: One possibility is the redistribution of pinned magnetic flux within the sample, implying that the amount of pinned magnetic field within the sample is constant, only its distribution is modified on varying the temperature. This behavior would cause a similar fringe pattern, as described for a cylindrical (solenoid) coil in⁷⁶. Another possibility could be the reduction in pinned magnetic flux as a function of temperature. This keeps the shape of the fringe pattern unchanged, and only H_{trap} decreases. On increasing the temperature from 5 K to 15 K shown in figure 5 and in the corresponding line plots in figure 6, no significant change in radiographs is evidenced, indicating that the amount of pinned field is constant up to $T = 15$ K. At temperatures between $T = 25$ K and 31 K (just below T_c), a drastic change in the magnetic flux fringe pattern indicates a loss of field inside the sample. On warming up the sample above T_c to $T = 32$ K, fringe pattern disappears completely, and sample reaches a normal non-superconducting state.

D. Flux pinning behavior as a function of magnetic field

We further explore the flux pinning behavior as a function of externally applied magnetic field at $T = 5$ K. Similar procedure as described above is employed towards these measurements with $H_{\text{ext}} = 10$ mT, 20 mT and 30 mT. Figure 8 shows the measured radiographs as a function of field in 0° sample orientation. As a function of applied magnetic field, evolution of fringe pattern is observed. At higher magnetic field the fringe density increases, retaining the Gaussian shaped distribution of the field inside the sample. As expected, with increasing H_{ext} the number of flux line pinning the sample also increase. Similar behavior is observed for 90° sample orientation. The observation of Gaussian flux distribution inside the sample is contrasting to the critical state Bean model⁵. When the sample is cooled from above T_c in the presence of H_{ext} , the strong pinning centers trap the magnetic flux inside the sample in the normal state in the form of vortices with uniform flux distribution inside the sample. This distribution of vortices is determined by the balance between the Lorentz force of the screening supercurrent and the forces pinning the vortices to material defects/inhomogeneities. The Lorentz force drives these vortices toward the center of the sample, with their motion hindered by the pinning sites. If the external field is varied, the vortices leave or enter the superconductor through its boundary. Additionally, within the region where the driving forces are able to surmount the pinning forces, the vortices rearrange themselves into another metastable state, with re-establishment of the equilibrium at the boundary with respect to the external magnetic field.

These experimentally obtained radiographs in 0° sample orientation as a function of external magnetic field are compared with theoretically modelled magnetic field distribution (simulated ones), to analyze and correlate the neutron spin precession through the magnetic field in the sample. R. Engel-Herbert *et al.* describes the magnetic stray field calculation for rectangular shaped bar magnet⁸⁰. In the present study we extend this formalism to calculate the magnetic stray field for cylindrical geometry (shown in figure 9), assuming (for simplicity) homogeneous magnetization. The magnetic field $H(r)$ at a point r (outside the domain $= (x, y, z)$) with scalar field Φ is described as, $\vec{H}(\vec{r}) = -\vec{\nabla}\Phi(\vec{r})$. This results in Poisson equation with the solution including magnetization and integrating over cylindrical geometry,

$$\Phi(x, y, z) = -\frac{M_o}{4\pi} \frac{\partial}{\partial y} \int_{-y_b}^{y_b} \int_{-\sqrt{R^2-z_b}}^{\sqrt{R^2-z_b}} \int_{-R}^R dy_i dz_i dx_i \times \frac{1}{\sqrt{(x-x_i)^2 + (y-y_i)^2 + (z-z_i)^2}} \quad (2)$$

Further, the correlated magnetic field dependent Larmor spin precession of polarized neutron beam transmitting

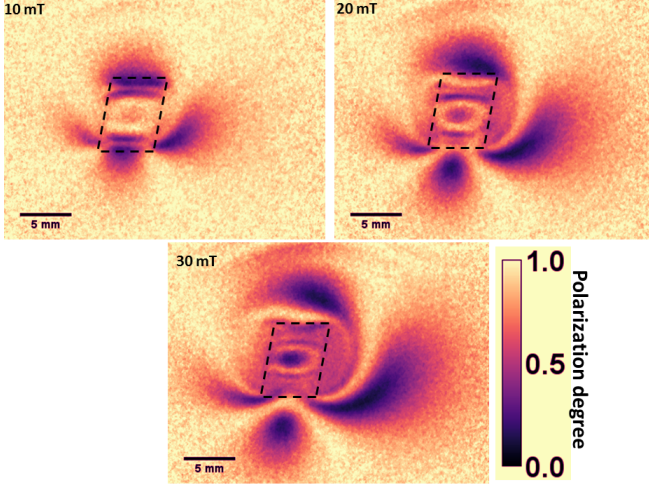


FIG. 8: Flux pinning behavior as a function of external magnetic field at $T = 5$ K for 0° orientation, for single crystal $\text{La}_{2-x}\text{Sr}_x\text{CuO}_4$ ($x = 0.09$) sample. Towards this, sample is cooled down to 5 K from room temperature, with applied magnetic field. At 5 K to visualize flux pinning, H_{ext} is switched off. The black dashed box indicates the sample and scale bar is 5 mm.

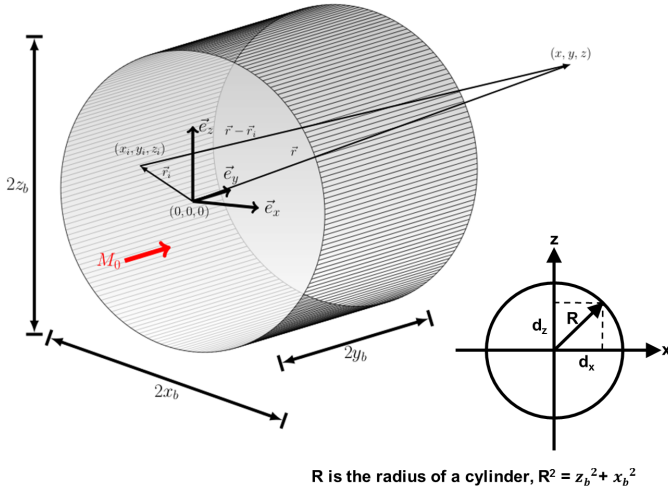


FIG. 9: Pictorial display of cylindrical geometry with integration limits is shown. Magnetization M is shown along y axis.

through the sample can be theoretically described by semi-classical spin rotation formalism^{81–83}. The change in polarization ($P(x)$) with respect to the incident polarized ($P(x_0)$) neutron beam (x is the neutron flight path direction) passing through a homogeneous magnetic field B , is given as,

$$\frac{\partial \overrightarrow{P(x)}}{\partial x} = A(x)P(x), \quad (3)$$

where,

$$A = \frac{\gamma L}{\nu} \begin{bmatrix} 0 & +B_z & -B_y \\ -B_z & 0 & +B_y \\ +B_y & -B_x & 0 \end{bmatrix} \quad (4)$$

and ν is the neutron velocity.

Therefore, change in polarization is given as,

$$P(x) = DP(x_0) \quad (5)$$

where, D (the rotation matrix) = $\exp[\int_{x_0}^x dx A(x)]$

Figure 10 displays (for 0° sample orientation) the calculated radiographs at various applied magnetic fields. While the figure 11 shows the corresponding line plots for clear comparison between calculated and experimentally obtained data at $H_{\text{ext}} = 30$ mT. To calculate the amount of flux pinned inside the sample, the magnitude of magnetic field that can be pinned inside sample is limited to H_{ext} . Similar features between calculated and experimental data are observed, as shown in figure 11. This indicates the possibility of external magnetic field completely pinned inside the sample. The calculated radiographs assume ideal system and conditions, with 100% degree of polarization, perfect instrument set-up, highly symmetrical and pure cylindrical geometry of the sample. However, in the experimental set up, limited instrument resolution, lower polarization degree (92%), imperfect sample geometry and, therefore inhomogeneity of pinned magnetic field is expected.

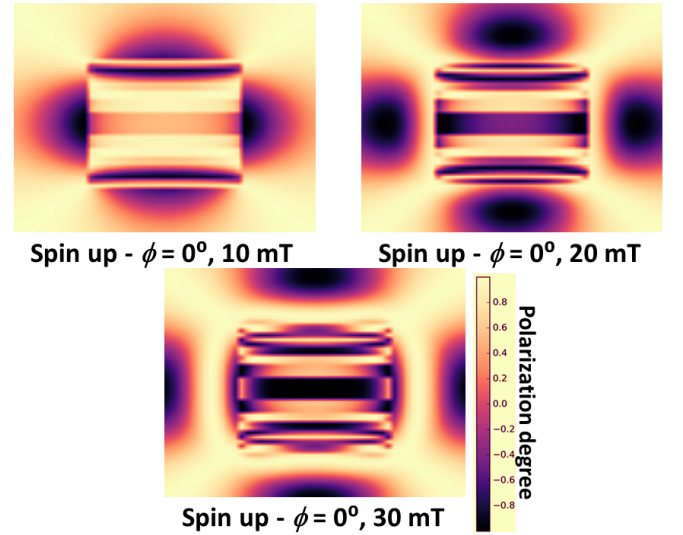


FIG. 10: Calculated flux pinning behavior for different values of external magnetic field for 0° orientation, compared with figure 8 for single crystal $\text{La}_{2-x}\text{Sr}_x\text{CuO}_4$ ($x = 0.09$) sample.

The phase diagram proposed in literature for $\text{La}_{2-x}\text{Sr}_x\text{CuO}_4$ series clearly shows the presence of competing superconducting and magnetic interactions as a function of Sr doping and / or the presence of excess oxygen^{13,14}. Similar behavior is also reported in other

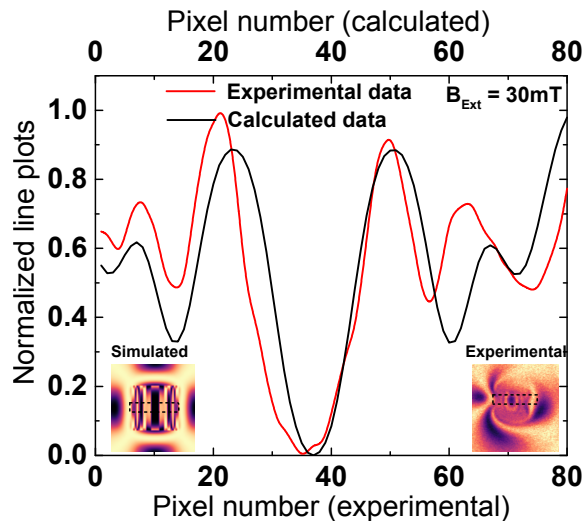


FIG. 11: The normalized line plot (for $H_{\text{ext}} = 30$ mT) showing the comparison between experimental ($T = 5$ K) and calculated radiographs at 0° orientation, for single crystal $\text{La}_{2-x}\text{Sr}_x\text{CuO}_4$ ($x = 0.09$) sample. Sum of the transmission intensity for each column as a function of pixel number is plotted. A region of interest selected for this plot is shown in the inset. Each pixel number corresponds to $78 \mu\text{m}$.

high T_c superconductors^{65–69}. The presence of these inhomogeneities can lead to strong and weak vortex pinning centers within the sample. It is possible that at low temperatures the magnetic flux lines pinned to these regions resist the movement. On increasing the temperature (Figure 5, at 25 K) the pinned magnetic flux begins to disappear from the weak pinning centers first. Eventually, complete disappearance of pinned magnetic flux (from both strong and weak vortex pinning centers) occurs at T_c . It would be of interest to further explore the distribution of flux pinning over the regions of several millimeter (sample size) to visualize the regions of high and low density of pinning centers in high- T_c superconductors for bulk samples using polarized neutron imaging technique.

V. CONCLUSION

Polarized neutron imaging study reveals the temperature and magnetic field dependent flux pinning be-

havior and Meissner effect for type - II single crystal $\text{La}_{2-x}\text{Sr}_x\text{CuO}_4$ ($x = 0.09$) superconductor. We observe signatures towards the existence of flux pinning behavior down to 5 K. Initially, for $5 \text{ K} \leq T \leq 15 \text{ K}$ magnetic fringes having Gaussian shaped distribution is visualized, implying pinned flux within the sample. As the temperature is increased to 25 K, non-uniformity in the flux distribution is seen. Further increase in temperature favors gradual reduction in pinned flux inside the sample, with sample attaining a normal state above T_c . Additionally, for Meissner phase with H_{ext} switched on, part of the applied magnetic field is expelled and part is pinned inside the sample. The flux pinning is further explored as a function of H_{ext} at $T = 5$ K. Evolution of fringe pattern is observed as a function of H_{ext} . With increasing magnetic field increase in fringe density is ascertained. Comparison between experimentally visualized and calculated pinned magnetic flux shows agreeable behavior, with quantification of pinned magnetic flux inside the bulk of a sample. In addition, the present study also demonstrates the potential of real space polarized neutron imaging technique for the visualization and quantification of the superconducting mixed state, particularly for high- T_c superconductors.

VI. ACKNOWLEDGEMENT

This material is based upon work supported by the U.S. Department of Energy, Office of Science, Office of Basic Energy Sciences, under contract number DE-AC05-00OR22725. We thank Helmholtz-Zentrum Berlin für Materialien und Energie GmbH for the allocation of neutron radiation beamtime. This work was supported by the Federal Ministry of Education and Research (BMBF) Project No 05K10KF1.

* email : idhiman@ornl.gov

¹ K. A. Müller and J. G. Bednorz, *The discovery of a class of high-temperature superconductors*, Science **237**, 1133 (1987).

² J. M. Tranquada, in *Handbook of High-Temperature Superconductivity*, edited by J. R. Schrieffer and J. S. Brooks (Springer, New York, 2007), pp. 257298.

³ J. Tranquada, in *Neutron Scattering in Layered Copper-Oxide Superconductors*, Edited by A. Furrer (Kluwer Academic, Dordrecht, 1998), p. 225.

⁴ G. Blatter, M. V. Feigelman, V. B. Geshkenbein, A. I. Larkin, and V. M. Vinokur, *Vortices in high-temperature superconductors*, Rev. Mod. Phys. **66**, 1125 (1994) and reference therein.

- ⁵ C. P. Bean, *Magnetization of High-Field Superconductors*, Rev. Mod. Phys. **36**, 31 (1964).
- ⁶ S. A. Kivelson, I. P. Bindloss, E. Fradkin, V. Oganessian, J. M. Tranquada, A. Kapitulnik and C. Howald, *How to detect fluctuating stripes in the high-temperature superconductors*, Rev. Mod. Phys. **75**, 1201 (2003), and reference therein.
- ⁷ J.-M. Tarascon, L. Greene, W. McKinnon, G. Hull, and T. Geballe, *Superconductivity at 40 K in the oxygen-defect perovskites $La_{2-x}Sr_xCuO_{4-y}$* , Science **235**, 1373 (1987).
- ⁸ H. Takagi, T. Ido, S. Ishibashi, M. Uota, S. Uchida, and Y. Tokura, *Superconductor-to-nonsuperconductor transition in $(La_{1-x}Sr_x)_2CuO_4$ as investigated by transport and magnetic measurements*, Phys. Rev. B **40**, 2254 (1989).
- ⁹ X. Shi, P. V. Lin, T. Sasagawa, V. Dobrosavljević, and D. Popović, *Two-stage magnetic-field-tuned superconductor insulator transition in underdoped $La_{2-x}Sr_xCuO_4$* , Nature Phys. **10**, 437 (2014).
- ¹⁰ M. Iavarone, S. Moore, J. Fedor, S. Ciocys, G. Karapetrov, J. Pearson, V. Novosad, and S. Bader, *Visualizing domain wall and reverse domain superconductivity*, Nature Commun. **5**, 4766 (2014).
- ¹¹ B. Keimer, N. Belk, R. J. Birgeneau, A. Cassanho, C. Y. Chen, M. Greven, M. A. Kastner, A. Aharony, Y. Endoh, R. W. Erwin, and G. Shirane, *Magnetic excitations in pure, lightly doped, and weakly metallic La_2CuO_4* , Phys. Rev. B **46**, 14034 (1992).
- ¹² M. A. Kastner, R. J. Birgeneau, G. Shirane, and Y. Endoh, *Magnetic, transport, and optical properties of monolayer copper oxides*, Rev. Mod. Phys. **70**, 897 (1998).
- ¹³ H. E. Mohottala, B. O. Wells, J. I. Budnick, W. A. Hines, C. Niedermayer, L. Udby, C. Bernhard, A. R. Moodenbaugh, and F.-C. Chou, *Phase separation in superoxygenated $La_{2-x}Sr_xCuO_{4+y}$* , Nature Mater. **5**, 377 (2006).
- ¹⁴ H. E. Mohottala, B. O. Wells, J. I. Budnick, W. A. Hines, C. Niedermayer, and F. C. Chou, *Flux pinning and phase separation in oxygen-rich $La_{2-x}Sr_xCuO_{4+y}$* , Phys. Rev. B **78**, 064504 (2008).
- ¹⁵ M. P. M. Dean, G. Dellea, R. S. Springell, F. Yakhov-Harris, K. Kummer, N. B. Brookes, X. Liu, Y. J. Sun, J. Strle, T. Schmitt, L. Braicovich, G. Ghiringhelli, I. Bozovic, and J. P. Hill, *Persistence of magnetic excitations in $La_{2-x}Sr_xCuO_4$ from the undoped insulator to the heavily over-doped non-superconducting metal*, Nature Mater. **12**, 1019 (2013).
- ¹⁶ A. Gozar, G. Logvenov, L. F. Kourkoutis, A. Bollinger, L. Giannuzzi, D. Muller, and I. Bozovic, *High-temperature interface superconductivity between metallic and insulating copper oxides*, Nature **455**, 782 (2008).
- ¹⁷ A. T. Bollinger, G. Dubuis, J. Yoon, D. Pavuna, J. Misewich, and I. Božović, *Superconductor-insulator transition in $La_{2-x}Sr_xCuO_4$ at the pair quantum resistance*, Nature **472**, 458 (2011).
- ¹⁸ B. Keimer, S. A. Kivelson, M. R. Norman, S. Uchida and J. Zaanen, *From quantum matter to high-temperature superconductivity in copper oxides*, Nature **518**, 179 (2015).
- ¹⁹ B. O. Wells, Y. S. Lee, M. A. Kastner, R. J. Christianson, R. J. Birgeneau, K. Yamada, Y. Endoh, G. Shirane, *Incommensurate Spin Fluctuations in High Transition Temperature Superconductors*, Science **277**, 1067 (1997).
- ²⁰ G. S. Boebinger, Y. Ando, A. Passner, T. Kimura, M. Okuya, J. Shimoyama, K. Kishio, K. Tamasaku, N. Ichikawa and S. Uchida *Insulator-to-metal crossover in the normal state of $La_{2-x}Sr_xCuO_4$ near optimum doping*, Phys. Rev. Lett. **77**, 5417 (1996).
- ²¹ W. Buckel and R. Kleiner, *Supraleitung*, 7th edition (Wiley-VCH Verlag).
- ²² C. P. Poole Jr., H. A. Farach, R. J. Creswick, and R. Prozorov, *Superconductivity*, 2nd edition (Academic press, Amsterdam, 2007).
- ²³ J. D. Livingston and W. DeSorbo, *Superconductivity* vol. 2 ed R. D. Parks (New York, Dekker) p 1235.
- ²⁴ M. Tinkham, *Introduction to superconductivity* (Dover Books of physics, New York, 2004).
- ²⁵ R. P. Huebener, *Magnetic flux structures in superconductors* (Springer-verlag, New York, 2001).
- ²⁶ J. L. MacManus-Driscoll, S. R. Foltyn, Q. X. Jia, H. Wang, A. Serquis, L. Civale, B. Maiorov, M. E. Hawley, M. P. Maley and D. E. Peterson, *Strongly enhanced current densities in superconducting coated conductors of $YBa_2Cu_3O_{7-x} + BaZrO_3$* , Nat. Mater. **3** 439 (2004).
- ²⁷ T. Haugan, P. N. Barnes, R. Wheeler, F. Meisenkothen and M. Sumption, *Addition of nanoparticle dispersions to enhance flux pinning of the $YBa_2Cu_3O_{7-x}$ superconductor*, Nature **430**, 867 (2004).
- ²⁸ A.M. Campbell and D.A. Cardwell, *Bulk high temperature superconductors for magnet applications*, Cryogenics **37**, 567 (1997).
- ²⁹ R.M. Scanlan, A.P. Malozemoff, and D.C. Larbalestier, *Superconducting materials for large scale applications*, Proc. IEEE **92**, 1639 (2004).
- ³⁰ J. H. Durrell, A. R. Dennis, J. Jaroszynski, M. D. Ainslie, K. G. B. Palmer, Y.-H. Shi, A. M. Campbell, J. Hull, M. Strasik, E. E. Hellstrom and D. A. Cardwell, *A trapped field of 17.6 T in melt-processed, bulk Gd-Ba-Cu-O reinforced with shrink-fit steel*, Supercond. Sci. Technol. **27**, 082001 (2014).
- ³¹ D. Koelle, R. Kleiner, F. Ludwig, E. Dantsker, and John Clarke, *High-transition-temperature superconducting quantum interference devices*, Rev. Mod. Phys. **71** 631 (1999).
- ³² M. Fujita, H. Hiraka, M. Matsuda, M. Matsuura, J. M. Tranquada, S. Wakimoto, G. Xu and K. Yamada, *Progress in Neutron Scattering Studies of Spin Excitations in High-Tc Cuprates*, J. Phys. Soc. Japan **81**, 011007 (2012) and references therein.
- ³³ L. Udby, N. H. Andersen, F. C. Chou, N. B. Christensen, S. B. Emery, K. Lefmann, J. W. Lynn, H. E. Mohottala, Ch. Niedermayer, and B. O. Wells, *Magnetic ordering in electronically phase-separated $La_{2-x}Sr_xCuO_{4+y}$: Neutron diffraction experiments*, Phys. Rev. B **80**, 014505 (2009).
- ³⁴ L. Udby, J. Larsen, N. B. Christensen, M. Boehm, Ch. Niedermayer, H. E. Mohottala, T. B. S. Jensen, R. Toft-Petersen, F. C. Chou, N. H. Andersen, K. Lefmann, and B. O. Wells, *Measurement of Unique Magnetic and Superconducting Phases in Oxygen-Doped High-Temperature Superconductors $La_{2-x}Sr_xCuO_{4+y}$* , Phys. Rev. Lett. **111**, 227001 (2013).
- ³⁵ N. B. Christensen, D. F. McMorrow, H. M. Rønnow, B. Lake, S. M. Hayden, G. Aeppli, T. G. Perring, M. Mangkorntong, M. Nohara, and H. Takagi, *Dispersive Excitations in the High-Temperature Superconductor $(La_{1-x}Sr_x)_2CuO_4$* , Phys. Rev. Lett. **93**, 147002 (2004).
- ³⁶ M. Kofu, S.-H. Lee, M. Fujita, H.-J. Kang, H. Eisaki, and K. Yamada, *Hidden Quantum Spin-Gap State in the Static Stripe Phase of High-Temperature $La_{2-x}Sr_xCuO_4$ Superconductors*, Phys. Rev. Lett. **102**, 047001 (2009).
- ³⁷ V. Vignolle, S. M. Hayden, D. F. McMorrow, H. M. Rønnow, B. Lake, C. D. Frost and T. G. Perring, *Two en-*

- ergy scales in the spin excitations of the high-temperature superconductor $La_{2-x}Sr_xCuO_4$, *Nature Phys.* **3**, 163 (2007).
- ³⁸ T. Suzuki, T. Goto, K. Chiba, T. Shinoda, T. Fukase, H. Kimura, K. Yamada, M. Ohashi, and Y. Yamaguchi, *Observation of modulated magnetic long-range order in $La_{1.88}Sr_{0.12}CuO_4$* , *Phys. Rev. B* **57**, R3229 (1998).
- ³⁹ H. Kimura, Kazuma Hirota, Hiroki Matsushita, Kazuyoshi Yamada, Yasuo Endoh, Seung-Hun Lee, Charles F. Majkrzak, Ross Erwin, Gen Shirane, Martin Greven, Young S. Lee, Marc A. Kastner, and Robert J. Birgeneau, *Neutron-scattering study of static antiferromagnetic correlations in $La_{2-x}Sr_xCu_{1-y}Zn_yO_4$* , *Phys. Rev. B* **59**, 6517 (1999).
- ⁴⁰ H. Kimura, H. Matsushita, K. Hirota, Y. Endoh, K. Yamada, G. Shirane, Y. S. Lee, M. A. Kastner, and R. J. Birgeneau, *Incommensurate geometry of the elastic magnetic peaks in superconducting $La_{1.88}Sr_{0.12}CuO_4$* , *Phys. Rev. B* **61**, 14366 (2000).
- ⁴¹ S. Katano, Masugu Sato, Kazuyoshi Yamada, Takao Suzuki, and Tetsuo Fukase, *Enhancement of static antiferromagnetic correlations by magnetic field in a superconductor $La_{2-x}Sr_xCuO_4$ with $x = 0.12$* , *Phys. Rev. B* **62**, R14677 (2000).
- ⁴² S. Wakimoto, G. Shirane, Y. Endoh, K. Hirota, S. Ueki, K. Yamada, R. J. Birgeneau, M. A. Kastner, Y. S. Lee, P. M. Gehring, and S. H. Lee, *Observation of incommensurate magnetic correlations at the lower critical concentration for superconductivity in $La_{2-x}Sr_xCuO_4$ ($x = 0.05$)*, *Phys. Rev. B* **60**, R769 (1999);
- ⁴³ S. Wakimoto, R. J. Birgeneau, M. A. Kastner, Y. S. Lee, R. Erwin, P. M. Gehring, S. H. Lee, M. Fujita, K. Yamada, Y. Endoh, K. Hirota, and G. Shirane, *Direct observation of a one-dimensional static spin modulation in insulating $La_{1.95}Sr_{0.05}CuO_4$* , *Phys. Rev. B* **61**, 3699 (2000);
- ⁴⁴ M. Matsuda, M. Fujita, K. Yamada, R. J. Birgeneau, M. A. Kastner, H. Hiraka, Y. Endoh, S. Wakimoto, and G. Shirane, *Static and dynamic spin correlations in the spin-glass phase of slightly doped $La_{2-x}Sr_xCuO_4$* , *Phys. Rev. B* **62**, 9148 (2000).
- ⁴⁵ S. Wakimoto, R. J. Birgeneau, Y. S. Lee, and G. Shirane, *Hole concentration dependence of the magnetic moment in superconducting and insulating $La_{2-x}Sr_xCuO_4$* , *Phys. Rev. B* **63**, 172501 (2001).
- ⁴⁶ M. Fujita, K. Yamada, H. Hiraka, P. M. Gehring, S. H. Lee, S. Wakimoto, and G. Shirane, *Static magnetic correlations near the insulating-superconducting phase boundary in $La_{2-x}Sr_xCuO_4$* , *Phys. Rev. B* **65** 064505 (2002).
- ⁴⁷ B. Lake, H. M. Rønnow, N. B. Christensen, G. Aeppli, K. Lefmann, D. F. McMorrow, P. Vorderwisch, P. Smeibidl, N. Mangkorntong, T. Sasagawa, M. Nohara, H. Takagi and T. E. Mason, *Antiferromagnetic order induced by an applied magnetic field in a high-temperature superconductor*, *Nature* **415**, 299 (2002).
- ⁴⁸ T. Reimann, S. Mühlbauer, M. Schulz, B. Betz, A. Kaestner, V. Pipich, P. Bönnini and C. Grünzweig, *Visualizing the morphology of vortex lattice domains in a bulk type-II superconductor*, *Nat. Commun.* **6**, 8813 (2015).
- ⁴⁹ S. Mühlbauer, C. Pfleiderer, P. Böni, M. Laver, E. M. Forgan, D. Fort, U. Keiderling, and G. Behr, *Morphology of the superconducting vortex lattice in ultrapure niobium*, *Phys. Rev. Lett.* **102**, 136408 (2009).
- ⁵⁰ M. Laver, C. J. Howell, E. M. Forgan, A. B. Abrahamsen, D. Fort, C. D. Dewhurst, S. Mühlbauer, D. K. Christen, J. Kohlbrecher, R. Cubitt, and S. Ramos, *Structure and degeneracy of vortex lattice domains in pure superconducting niobium: A small-angle neutron scattering study*, *Phys. Rev. B* **79**, 014518 (2009).
- ⁵¹ S. Mühlbauer, C. Pfleiderer, P. Böni, E. M. Forgan, E. H. Brandt, A. Wiedenmann, U. Keiderling, and G. Behr, *Time resolved stroboscopic neutron scattering of vortex lattice dynamics in superconducting niobium*, *Phys. Rev. B* **83**, 184502 (2011).
- ⁵² A. Pautrat, and A. Brûlet, *Temperature dependence of clusters with attracting vortices in superconducting niobium studied by neutron scattering*, *J. Phys. Condens. Matter* **26**, 232201 (2014).
- ⁵³ D. K. Christen, F. Tasset, S. Spooner, and H. A. Mook, *Study of the intermediate mixed state of niobium by small-angle neutron scattering*, *Phys. Rev. B* **15**, 4506 (1977).
- ⁵⁴ Simon J. Bending, *Local magnetic probes of superconductors*, *Advances in Physics*, **48**, 449 (1999).
- ⁵⁵ Ilija Zeljkovic, Elizabeth J. Main, Tess L. Williams, M. C. Boyer, Kamallesh Chatterjee, W. D. Wise, Yi Yin, Martin Zech, Adam Pivonka, Takeshi Kondo, T. Takeuchi, Hiroshi Ikuta, Jinsheng Wen, Zhijun Xu, G. D. Gu, E.W. Hudson and Jennifer E. Hoffman, *Scanning tunnelling microscopy imaging of symmetry-breaking structural distortion in the bismuth-based cuprate superconductors*, *Nat. Mater.*, **11**, 585 (2012).
- ⁵⁶ J. R. Kirtley, *Fundamental studies of superconductors using scanning magnetic imaging*, *Rep. Prog. Phys.* **73** 126501 (2010) and reference therein.
- ⁵⁷ Øystein Fischer, Martin Kugler, Ivan Maggio-Aprile, Christophe Berthod and Christoph Renner, *Scanning tunneling spectroscopy of high-temperature superconductors*, *Rev. Mod. Phys.*, **79**, 353 (2007).
- ⁵⁸ H. Suderow, I. Guillamón, J. G. Rodrigo, and S. Vieira, *Imaging superconducting vortex cores and lattices with a scanning tunneling microscope*, *Supercond. Sci. Technol.* **27**, 063001(2014)
- ⁵⁹ Jennifer E. Hoffman, *Spectroscopic scanning tunneling microscopy insights into Fe-based superconductors*, *Rep. Prog. Phys.* **74** 124513 (2011).
- ⁶⁰ Ch Jooss, J. Albrecht, H. Kuhn, S. Leonhardt and H. Kronmüller, *Magneto-optical studies of current distributions in high- T_C superconductors*, *Rep. Prog. Phys.* **65** 651 (2002), and references therein.
- ⁶¹ R. Prozorov, R. W. Giannetta, A. A. Polyanskii, and G. K. Perkins, *Topological hysteresis in the intermediate state of type-I superconductors*, *Phys. Rev. B* **72**, 212508 (2005).
- ⁶² R. Prozorov, *Equilibrium Topology of the Intermediate State in Type-I Superconductors of Different Shapes*, *Phys. Rev. Lett.* **98**, 257001 (2007).
- ⁶³ R. Prozorov, A. F. Fidler, J. R. Hoberg, and P. C. Canfield, *Supraflow in type-I superconductors*, *Nat. Phys.* **4**, 327 (2008).
- ⁶⁴ A. Finkler, D. Vasyukov, Y. Segev, L. Néeman, E. O. Lachman, M. L. Rappaport, Y. Myasoedov, E. Zeldov, and M. E. Huber, *Scanning superconducting quantum interference device on a tip for magnetic imaging of nanoscale phenomena*, *Rev. Sci. Instrum.* **83**, 073702 (2012).
- ⁶⁵ K. Harada, O. Kamimura, H. Kasai, T. Matsuda, A. Tonomura, V. V. Moshchalkov, *Observation of Dynamic Interaction of Vortices with Pinning Centers by Lorentz Microscopy*, *Science*, **271** 1393 (1996).
- ⁶⁶ A. Tonomura, H. Kasai, O. Kamimura, T. Matsuda, K. Harada, J. Shimoyama, K. Kishio, and K. Kitazawa, *Motion of vortices in superconductors*, *Nature* **397**, 308

- (1999).
- ⁶⁷ A. Tonomura, H. Kasai, O. Kamimura, T. Matsuda, K. Harada, T. Yoshida, T. Akashi, J. Shimoyama, K. Kishio, T. Hanaguri, K. Kitazawa, T. Masui, S. Tajima, N. Koshizuka, P. L. Gammel, D. Bishop, M. Sasase, and S. Okayasu, Observation of Structures of Chain Vortices Inside Anisotropic High-Tc Superconductors, *Phys. Rev. Lett.* **88**, 237001 (2002).
- ⁶⁸ K. Harada, T. Matsuda, J. Bonevich, M. Igarashi, S. Kondo, G. Pozzi, U. Kawabe And A. Tonomura, *Real-time observation of vortex lattices in a superconductor by electron microscopy*, *Nature* **360**, 51 (1992).
- ⁶⁹ K. Harada, *Lorentz microscopy observation of vortices in high-Tc superconductors using a 1-MV field emission transmission electron microscope*, *Microscopy* **62**(Suppl. 1), S3 (2013).
- ⁷⁰ W. Treimer, *Radiography and tomography with polarized neutrons*, *J. Magn. Magn. Mater.* **350**, 188 (2014).
- ⁷¹ K. Kishio, Y. Nakayama, N. Motohira, T. Noda, T. Kobayashi, K. Kitazawa, K. Yamafuji, I. Tanaka and H. Kojima, *Anisotropic Magnetization, Flux Pinning and Critical Current Density of La-Sr-Cu-O Single Crystal*, *Supercond. Sci. Technol.* **5**, S69 (1992).
- ⁷² N. Kardjilov, I. Manke, M. Strobl, A. Hilger, W. Treimer, M. Meissner, T. Krist, and John Banhart, *Three-dimensional imaging of magnetic fields with polarized neutrons*, *Nat. Phys.* **4**, 399 (2008).
- ⁷³ M. Dawson, I. Manke, N. Kardjilov, A. Hilger, M. Strobl, and J. Banhart, *Imaging with polarized neutrons*, *New J. Phys.* **11**, 043013 (2009).
- ⁷⁴ M. Schulz, A. Neubauer, P. Böni, C. Pfeleiderer, *Neutron depolarization imaging of the hydrostatic pressure dependence of inhomogeneous ferromagnets*, *Appl. Phys. Lett.* **108**, 202402 (2016).
- ⁷⁵ A. S. Tremsin, N. Kardjilov, M. Strobl, I. Manke, M. Dawson, J. B. McPhate, J. V. Vallerga, O. H. W. Siegmund, and W. B. Feller, *Imaging of dynamic magnetic fields with spin-polarized neutron beams*, *New J. Phys.* **17**, 043047 (2015).
- ⁷⁶ W. Treimer, O. Ebrahimi, N. Karakas and R. Prozorov, *Polarized neutron imaging and three-dimensional calculation of magnetic flux trapping in bulk of superconductors*, *Phys. Rev. B* **85**, 184522 (2012).
- ⁷⁷ I. Dhiman, O. Ebrahimi, N. Karakas, H. Hoppner, R. Ziesche, and, W. Treimer, *Role of temperature on flux trap behavior in < 100 > Pb Cylindrical sample: Polarized neutron radiography investigation*, *Phys. Proc.* **69**, 420 (2015).
- ⁷⁸ W. Treimer, O. Ebrahimi, and N. Karakas, S. O. Seidel, *PONTO - An instrument for imaging with polarized neutrons*, *Nucl. Instrum. Methods Phys. Res., Sect. A* **651**, 53 (2011).
- ⁷⁹ E. H. Brandt, *Geometric barrier of superconductors with and without pinning*, *Physica B* **284-288** 743 (2000).
- ⁸⁰ R. Engel-Herbert, and T. Hesjedal, *Calculation of the magnetic stray field of a uniaxial magnetic domain*, *J. Appl. Phys.* **97**, 074504 (2005).
- ⁸¹ H. Leeb, M. Hochhold, G. Badurek, R. J. Buchelt and A. Schricker, *Neutron magnetic tomography: a feasibility study*, *Aust. J. Phys.* **51**, 401 (1998).
- ⁸² G. Badurek, M. Hochhold, and H. Leeb, *Neutron magnetic tomography A novel technique*, *Physica B: Condensed Matter* **234**, 1171 (1997).
- ⁸³ M. Th. Rekveldt, *Study of ferromagnetic bulk domains by neutron depolarization in three dimensions*, *Z. Phys.* **259**, 391 (1973), M. Th. Rekveldt, *Correlations in ferromagnetic domain structures studied by means of the neutron depolarization technique*, *J. Magn. Magn. Mater.* **1**, 342 (1976).
- ⁸⁴ M. Terasawa, N. Takezawa, K. Fukushima, T. Mitamura, X. Fan, H. Tsubakino, T. Kohara, K. Ueda, Y. Awaya, T. Kambara, M. Matsuda, G. Tatara, *Flux pinning and flux creep in La_{2-x}Sr_xCuO₄ with splayed columnar defects*, *Physica C* **296**, 57 (1998).